Semantic 3D Reconstruction of Furnished Interiors using Laser Scanning and RFID Technology

SEMANTIC 3D RECONSTRUCTION OF FURNISHED INTERIORS USING LASER SCANNING AND RFID TECHNOLOGY

Enrique Valero, Ph.D.; [1] Antonio Adán, Ph.D. [2] and Frédéric Bosché, Ph.D. [3]

ABSTRACT

Terrestrial Laser Scanning (TLS) technology is increasingly used for the generation of accurate 3D models of objects and scenes. But, converting the acquired 3D point cloud data into a representative, semantic 3D model of the scene requires advanced processing and skills. This research field is challenging, particularly when considering inhabited, furnished environments that are characterised by clutter and occlusions. This paper presents a TLS data processing pipeline aimed at producing semantic 3D models of furnished office and home interiors. The structure of rooms (floor, ceiling, and walls with window and door openings) is created using Boundary Representation (B-Rep) models, that not only encode the geometry of those elements, but also their connectivity. Windows and doors are recognized and modelled using a novel method based on molding detection. For the furniture, the approach uniquely integrates smart technology (RFID) that is increasingly used for Facilities Management (FM). RFID tags attached to furniture are sensed at the same time as laser scanning is conducted. The collected IDs are used to retrieve discriminatory geometric information about those objects from the building's FM database, that this information is used to support their recognition and modeling in the point cloud data. The manuscript particularly reports results for the recognition and modeling of chairs, tables and wardrobes (and other similar objects like chest of drawers). Extended experimentation of the method has been carried out in real scenarios yielding encouraging results.

Keywords: 3D laser scanner, 3D data processing, RFID, B-Rep model, Building Information Modeling

INTRODUCTION

Terrestrial Laser Scanning (TLS) technology is increasingly used for the generation of accurate 3D models of objects and scenes. While the technology has application in numerous fields such as cultural heritage or forensics, this article focuses on its application in the Architecture, Engineering, Construction and Facilities Management (AEC/FM) industry. In the AEC/FM sector, a particular area of interest for the application of such systems is the synthesis of 3D Building Information Modeling (BIM) models of buildings, facilities or infrastructure.

The wide majority of systems reported to date, academic research or commercial software, focuses on the modeling of building or room structural components, with far fewer works tackling the automatic generation of 3D (BIM) models for furnished (i.e. inhabited) rooms, houses and buildings. Yet, there are applications that require 3D models of interiors that contain not just

[1]Research Associate. School of Energy, Geoscience, Infrastructure and Society, Heriot-Watt University, Edinburgh EH14 4AS, United Kingdom. E-mail: e.valero@hw.ac.uk. Corresponding author

[2]Associate Professor. 3D Visual Computing and Robotics Lab, Universidad de Castilla-La Mancha, 13005 Ciudad Real, Spain. E-mail: antonio.adan@uclm.es.

[3]Lecturer. School of Energy, Geoscience, Infrastructure and Society, Heriot-Watt University, Edinburgh EH14 4AS, United Kingdom. E-mail: f.n.bosche@hw.ac.uk.

their structure (floor, ceiling and walls, with openings like doors and windows), but also their furniture, and possibly even other smaller objects. These particularly include applications based on robot navigation and robot interaction with the environment (grasping, pushing, moving) (Srinivasa et al. 2008). One such field of application, for which interest is currently growing rapidly, is the use of robots for supporting elderly or handicap people in their homes (Mast et al. 2012). Other applications include: conducting security inspections; conducting inventories (Ehrenberg et al. 2007); or situations when there is the presence of hazards for humans, for example when navigating buildings after earthquakes (Wandel et al. 2003; Marques et al. 2002; Ishida et al. 2004).

The complete 3D reconstruction of interior scenes from point cloud data, that is the reconstruction of 3D models where the structure and furniture are both precisely modeled, is a complex task at two levels:

- Furniture creates clutter and occlusion that challenge algorithms for recognizing and modeling the structure of rooms.
- Furniture can have a wide range of shape and is movable, meaning that little prior information can be used regarding their potential location in the room.

Accordingly, this paper presents a unique system for the automatic generation of 3D models of inhabited interiors, by means of TLS and Radio-Frequency IDentification (RFID) technology. The use of RFID technology is motivated by the fact that it is increasingly used for application in Facilities Managements (FM) where objects (especially mobile ones like furniture) are tagged for simplifying their identification — see (Lu et al. 2011) for a broad review of applications of RFID in this field. Furthermore, recent BIM developments such as the NBS National BIM Library `http://www.nationalbimlibrary.com/` (see also the Polantis Ikea 3D model database at `http://www.polantis.com/ikea`) will inevitably lead to FM databases containing detailed 3D models of all objects, including furniture, contained in buildings.

Figure 1 illustrates an example of scenes dealt with in this paper, with the point cloud acquired by the scanner and the final 3D interior model produced by our system.

The rest of the article is organized as follows. Some of the most significant and relevant works in the field of modeling from 3D point clouds are reviewed in Sections *Modeling from 3D point clouds* and *TLS and RFID integration: motivation and contribution*, with particular focus on applications in the AEC/FM sector. Our proposed approach is then described in Section *Method*. Section *Experimental Results* presents experimental results demonstrating its performance. Finally, Section *Conclusions* presents the conclusions and future works.

MODELING FROM 3D POINT CLOUDS

Dense raw data provided by laser scanners are typically processed manually or semi-automatically by engineers to create 3D models. These models range from mesh and CAD models in which components are considered as individual geometric elements, are not explicitly classified and do not include connectivity information, to BIM models in which the objects have all this information, and possibly more (e.g. material, energy performance).

In the last few years, commercial solutions have emerged that enable the creation of 3D models, a process now commonly called *as-is modelling*. A basic solution is for example provided by Matterport (`http://matterport.com/`) that uses proprietary 3D cameras to create 3D point clouds and meshes of indoor environments. This solution however does not tackle the automatic recognition and/or segmentation of the different scanned components for the creation of

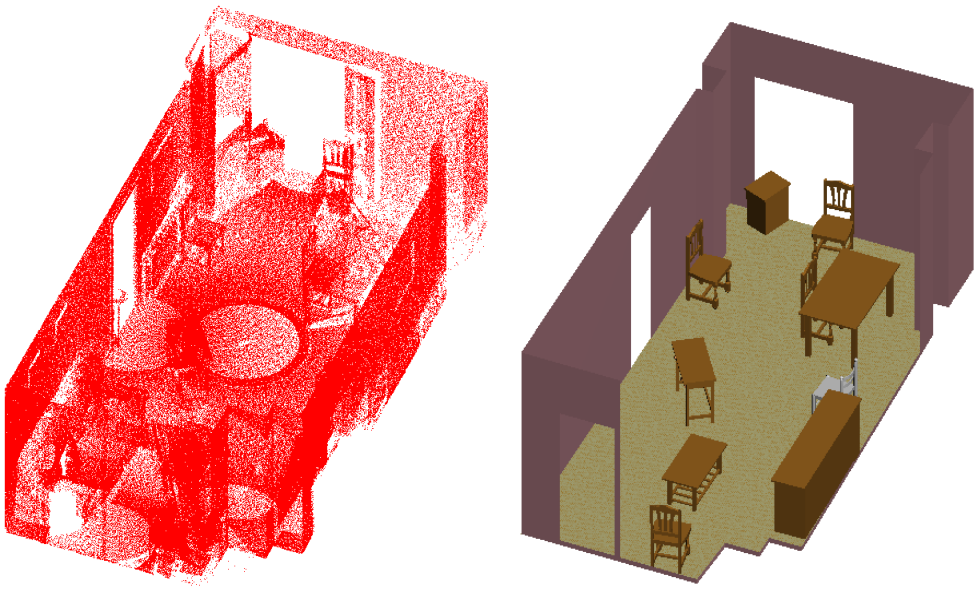

FIG. 1. Point cloud and the produced 3D model.

semantically-rich models. More advanced software solutions are also available for the modelling of 3D CAD/BIM models from TLS point clouds. For example, ClearEdge3D™ (`http://www.clearedge3d.com/`) commercializes the EdgeWise Building™ software package that features functionalities for (semi-) automatically extracting structural components like walls, windows, doors from TLS point clouds and exporting them in a BIM model format. This can be considered an example of the current state-of-the-art commercial solutions for structural modelling of interiors. Yet, the software does not consider the modelling of furniture, and in fact may require that rooms be as empty as possible when scanned so that point clouds are acquired from the entire surface of the structural components.

From a research viewpoint, different approaches dealing with the creation of realistic non-parametric models have been proposed over the last decades. Some of these focus on outdoor environments, others on interiors.

As regards the modeling of building exteriors, Frueh et al. (2005) and Bohm (2008) present different algorithms for reconstructing façades from 3D laser scanned data and images. Remondino et al. (2009) propose a combination of measurement techniques for the virtual reconstruction of complex architectures. In (Pu and Vosselman 2009), a region-growing algorithm is proposed that aims to segment windows, doors and roofs in outdoor façades with overall flat surfaces. More recently, Wang et al. (2015) have proposed a method for extracting structural geometries (such as roofs, walls, doors and windows) from unorganized point clouds.

Interior environments are delimited by structural, immobile components, such as floors, ceilings and walls with windows and doors, that enclose the environment and provide the boundaries of the scene. Typical inhabited interior environments also contain other objects, particularly furniture. The difficulty regarding the reconstruction of such environments arises from the presence of that furniture (and other objects) that can have various shapes, creates disorder, occludes the walls and other components during scanning. Many researchers have focused their attention on the

recognition and modelling of particular parts of the building structure of interior spaces, such as walls, columns, and doors, as well as specific furniture. El-Hakim et al. (1997) present a mobile mapping system to generate 3D models of indoor environments using a combination of location tracking and 2D range imaging devices. Stamos and Allen (2000) present an approach to generate large planar areas with primitives and non-planar areas with dense mesh elements. Plane sweep approaches have also been widely investigated to find planar regions and define the walls in a point cloud of a room (Hahnel et al. 2003; Budroni and Bohm 2005). Kwon et al. (2004) recognize different objects by automatically fitting elementary geometric shapes (cuboids, cylinders and spheres) to point clouds. Okorn et al. (2010) present an automatic method to generate precise 2D plans for indoors and Adán and Huber (2011) propose a solution based on region labelling to reconstruct interior boundaries. Valero et al. (2012b) present a method that automatically yields Boundary Representation (B-Rep) models of the structure of interiors (floor, ceiling and walls) from dense TLS point clouds. Interestingly, the B-Rep representation enables the modeling of not only the surface geometry of each objects, but also their connectivity. Recently, Dimitrov and Golparvar-Fard (2015) presented a robust algorithm for segmenting point cloud into smooth surfaces. While the work does not address the actual recognition and modelling of building components, the segmented surfaces would provide a valuable basis for it. Ali et al. (2008) identify windows by means of boundary analysis in binary images and texture information.

In relation to the specific problem of 3D reconstruction from partial data due to occlusions, Dell Acqua and Fisher (2002) present a method to reconstruct planar surfaces located behind objects which occlude them. Xiong et al. (2013) detect and model the main structural components of an indoor environment (floors, ceilings, and walls) including windows and doorways despite the presence of significant clutter and occlusion.

Other approaches relate to our work by their consideration for prior knowledge about the analysed scanned scene. For example, Bosché (2010), Anil et al. (2013) and Kim et al. (2013) identify components in built environments using the valuable information contained in existing (e.g. as-designed) 3D models.

The rapid development of inexpensive solutions to generate 3D point clouds, such as RGB-D cameras, has encouraged many researchers, mainly in the field of computer vision, to employ these devices to capture and rapidly understand and model indoor environments. For example, Guo and Hoiem (2013) tackle the identification of horizontal and planar surfaces that can support objects and people (such as chairs, beds and tables) from single RGB-D images. Silberman et al. (2012) present an algorithm to segment RGB-D data into surfaces and object regions and infer their structural and 'support' topology. Jia et al. (2013) segment different small objects, such as books or boxes, in indoor scenes but these are simply modelled as cuboids. And finally, in (Xiao et al. 2013), an object labelling tool for inhabited interiors is presented.

However, these authors note that, while all these approaches manage to recognize and model the main structural elements of rooms (floor, ceiling and walls), they only provide coarse segmentations of the 'foreground' objects typically into basic classes such as 'furniture' and 'clutter'. They do not address the problem of precisely recognizing and modeling individual pieces of furniture.

It is interesting to note that very little work has been published on the detection and modelling of furniture. Looking at all the approaches reviewed above, none of them considers the precise recognition and modeling of furniture beyond the coarse labelling of data regions as 'furniture' or

'clutter'. Relevant works in this area include that of Rusu et al. (2008) who identify pieces of furniture and utensils in point clouds of a corner of a kitchen. Wang and Oliveira (2002) take advantage of the symmetry of certain objects to reconstruct them when they are affected by occlusion. And Castellani et al. (2002) work on the reconstruction of corners and edges of furniture that is partially occluded.

TLS AND RFID INTEGRATION: MOTIVATION AND CONTRIBUTION

From the literature reviewed above, it appears that none of the existing works on *as-is modeling* provides a complete solution for the reconstruction of semantically-rich models of interiors where both structural elements and furniture are precisely modelled. Indeed, while many of the approaches above are able to reconstruct the structure of interiors with detailed classification of the segmented regions (e.g. surfaces classified as walls, floor and ceiling), they generally only provide a coarse segmentation and classification of the rest of the interior objects (e.g. object classified as 'furniture' or 'clutter' without more precision).

In contrast, these researchers present a novel approach that achieves the reconstruction of semantic 3D models of inhabited, furnished interiors where both the structure and furniture are accurately and precisely segmented, classified and modelled in TLS point cloud data. The approach is geared towards the specific context where furniture is tagged with RFID tags that link each piece of furniture to additional relevant information stored in a Facilities Management (FM) database. While such context is arguably simpler, these authors have shown that it is also increasingly common to use smart technologies, like RFID technology, in construction and FM (Jaselskis et al. 1995; Lu et al. 2011).

While RFID technology has been widely discussed in the literature and is already used in industry for various applications, few papers relate RFID technology to 3D scene reconstruction and understanding. El-Omari and Moselhi (2011) have proposed to integrate RFID and TLS technologies to track the state of materials on jobsites, but they consider the two technologies at two different stages in the construction supply chain; RFID is not used to detect objects within TLS data. In contrast, the work of Cerrada et al. (2009) is more relevant as they use the information stored in smart tags to improve the performance of object recognition in laser scanned data. However, they deal with small scenarios with geometrical shapes laid on a table. It is also worth noting the work of Ehrenberg et al. (2007) who developed a mobile robot that conducts library inventory, where the robot is equipped with an RFID reader to identify the books present on the shelves.

In contrast, the authors focus on the 3D reconstruction of large building interiors, a problem for which the above-mentioned integration has not been considered to date. In a previous publication, these researchers have dealt with the creation of 3D models of interiors using RFID. In (Valero et al. 2012a), TLS and RFID technology are combined to obtain simple 3D models of inhabited interiors. Beside the building's structure, furniture is also recognized to generate simple semantic 3D models of interiors. However, that work did not consider other structural elements, such as interior 'free' columns, nor did it consider the recognition and modeling of wall openings such as doors and windows. For the identification and modeling of furniture, the algorithms behind the results in (Valero et al. 2012a) were not presented in detail and their performance was also not assessed in detail.

In this paper, that earlier work is extended in many ways:

- *Modelling of walls*: An improved algorithm is proposed that models wall planes more accurately.
- *Detection and Modelling of wall openings*: B-Rep models of interiors are completed with wall openings, such as windows and doorways, as well as interior 'free' columns. In particular, a novel algorithm is presented for the recognition of openings based on a molding detection.
- *Identification and modeling of furniture*: The algorithms that calculate the pose of furniture in the point cloud are improved and detailed.
- *Experimental validation*: Experimentation is extended to larger environments, and new assessment procedures are included that further demonstrate the strengths of the method.

METHOD

Overview

The flowchart of Figure 2 summarizes the strategy to create a 3D model of the scene. The elements that compose an inhabited interior are divided into two groups:

- *(Immobile) Structural elements*, that include the ceiling, floor, walls and columns, along with the main openings within the walls (windows and doors).
- *(Mobile) Furniture*, that include tables, chairs, and wardrobe-like objects.

First of all, it is assumed that 3D data acquisition and pre-processing (i.e. filtering and registration of multiple point clouds) have been carried out, leading to the point cloud labelled D_1 in Figure 2. Then, a sequential processing is applied where, at each consecutive stage, one type of element is automatically recognized (point set S_i), modelled and removed from the point cloud ($D_{i+1} = D_i - S_i$). This sequential strategy starts with structural elements — successively floor/ceiling, walls, columns, doors and windows — and then moves on to furniture — successively tables, chairs, wardrobes, and wastepaper baskets. Structural elements are detected using the 3D TLS data only, and the room's structure is modelled using a B-Rep representation that captures not only the geometry of the individual structural elements, but also their connectivity. Then, furniture is identified in the room by means of RFID tags attached to them and sensed by a reader mounted alongside the laser scanner. The IDs enable the retrieval from the building's FM database of relevant geometric information for the identified pieces of furniture (including their 3D models) that are used to accurately recognize and precisely model them in the TLS point cloud.

All these stages are detailed in the following sub-sections.

Modeling of room structure

In order to detect and model the structural elements from the point cloud data, the 3D space is first discretized in a uniform 3D voxel grid. This voxelization has two purposes: reduce computational complexity, and act as a noise filter. Then, the approach conducts the following successive steps:

1. Detect and model the data planes that contain the 3D points belonging to the boundary of the scene (i.e. floor, ceiling and walls).
2. Detect and model the data corresponding to interior 'free' columns
3. Detect and model openings in the wall corresponding to doors and windows.
4. Generate a complete semantic 3D model of the room's structure.

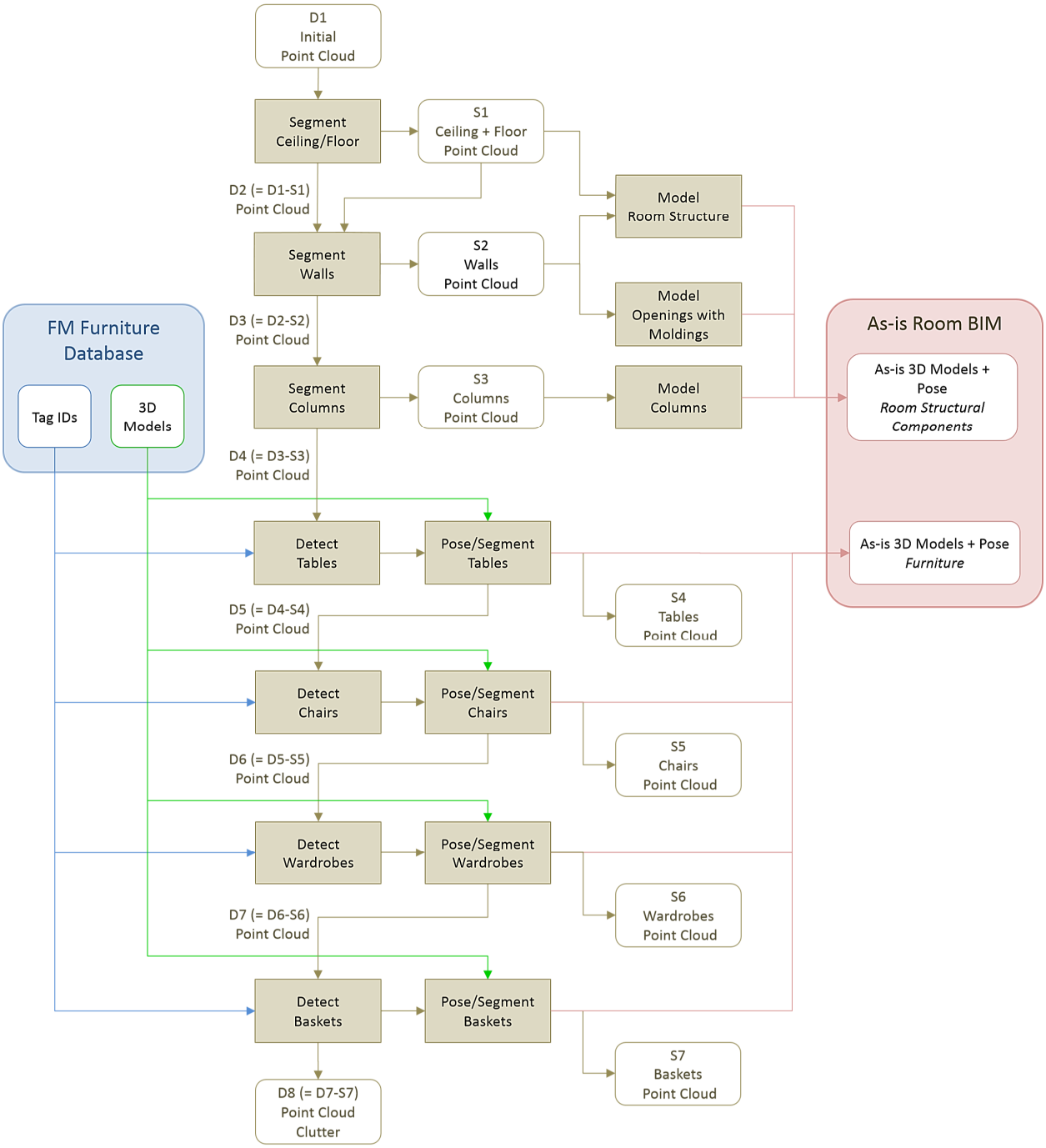

FIG. 2. Overview of the proposed data processing pipeline.

A detailed presentation of the overall approach to model the room structural boundary elements (ceiling, floor and walls) can be found in (Valero et al. 2012b). However, note that an improved method for modelling the walls is reported here. Also, steps 2 and 3 above constitute new contributions to the overall room structure modeling approach.

The processing steps above are presented in the following sub-sections. To support the presentation, an illustrative example, corresponding to a real case study, is used. Figure 3 shows a photo and the initial point cloud (D_1) of this illustrative interior room.

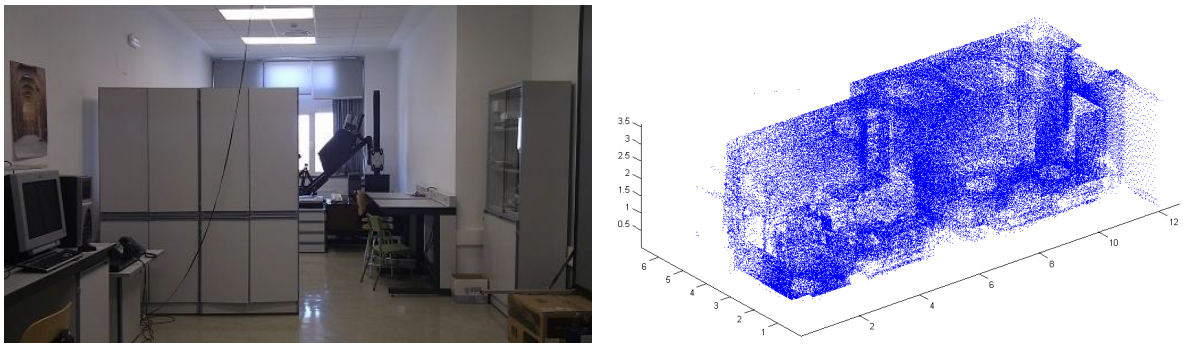

(a) Photo of the room.

(b) Initial TLS point cloud of the room.

FIG. 3. Example furnished interior used to illustrate the room structural modelling approach.

Floor and ceiling segmentation

Formally, the uniform voxel space can be defined in a universal coordinate system (UCS) by means of the voxel size ε and the 3D coordinates of each voxel's center (v_x, v_y, v_z). The voxel space's origin and voxel size are initially considered unknown and are collectively calculated with the detection of the floor and ceiling data planes.

The goal is then to produce a voxelization of the space that leads to most of the points belonging to the floor and ceiling being contained in thin parallelepipeds M_f and M_c of height ε (see Figure 4(a)). An integrated algorithm has been developed that automatically achieves this optimization; see (Valero et al. 2012a) for details. Figure 4(b) shows floor and ceiling segmentation results for the illustrative case. Note that this method assumes that the floor and ceiling are both horizontal; by far the common situation.

Wall segmentation

In rectangular indoor plans, the walls could be detected by adapting the process above to two pairs of parallel voxels planes. Instead, the authors consider the more complex case of the extraction of walls in arbitrary plans in which walls are designed to be straight, but not necessarily perpendicular or parallel to one another.

As illustrated in Figure 5, the authors propose to carry out the wall detection in a 'top view' 2D binary image, I, obtained by orthogonal projection of the entire initial 3D point cloud data (D_1) on a horizontal plane (Figure 5(a)). Pixels of I are labeled *occupied* (1) or *empty* (0) depending on whether TLS points fall within them (Figure 5(b)). I is used to detect the room boundary (walls) (Figure 5(c)). Then, a Hough Transform algorithm is applied to the dilated room boundary binary image to detect initial approximate locations and extents of the walls (Figure 5(d)). For each of the

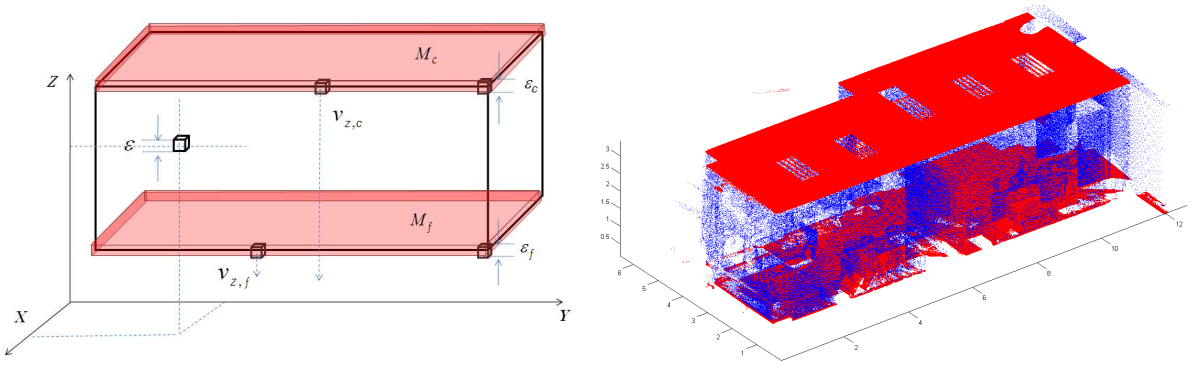

(a) Illustration of the process employed to simultaneously define the space voxelisation and segment the floor and ceiling points from the initial room point cloud.

(b) Results of the floor and ceiling segmentation.

FIG. 4. Illustration of the floor and ceiling segmentation process.

walls, a RANSAC (Fischler and Bolles 1981) -based algorithm is then used to calculate the plane equation that optimally fits the data while discarding outlier points (e.g. from objects positioned against the wall). Singular Value Decomposition (SVD), which provides the normal to the wall plane, is used to calculate the equation of the planes which best fit each wall. For each iteration, three points are randomly selected to calculate a plane equation and the plane support is calculated as the number of remaining points that satisfy a distance-to-plane threshold (e.g. according to DIN 18202 (Deutsches Institut fur Normung 2005)) and whose normal vector does not differ from that of the hypothesized wall plane by more than 15°. The plane leading to the largest support after 1,000 iterations is considered the best plane.

Figure 5(e) shows the resulting segmentation of points belonging to the walls for the illustrative case.

Room boundary B-Rep model

The floor, ceiling and wall detection and segmentation stages produce the planes corresponding to each one of those elements. The following step consists in converting this information into a unified surface representation. Among possible 3D representations, the B-Rep model (Mortenson 1985) has been chosen. In B-Rep, a shape is described by a set of surface elements along with connectivity information describing the topological relationships between the elements.

The floor, ceiling and wall plane equations directly correspond to *surfaces* in the B-Rep representation. Given the expected topological relationships between the different elements (each wall intersects the floor and the ceiling; the intersecting walls are known from the process defined in the previous section), the relevant intersections between planes are defined, yielding the *faces*, *edges* and *point* topological entities in the B-Rep. Figure 6 illustrates the B-Rep model obtained for the illustrative case.

Modeling of interior columns

Sets of points which precisely fit to vertical cylinders or parallelepipeds that span the entire height of the room are recognized as interior ‘free’ columns. This is achieved with the process detailed below and illustrated in Figure 7.

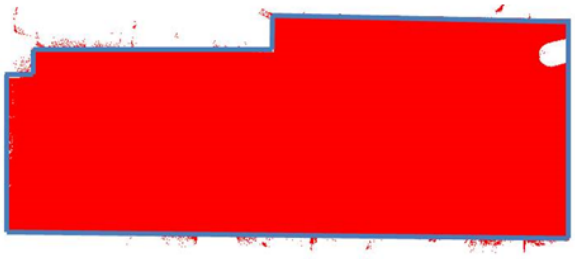

(a) Top view of the initial point cloud (D_1).

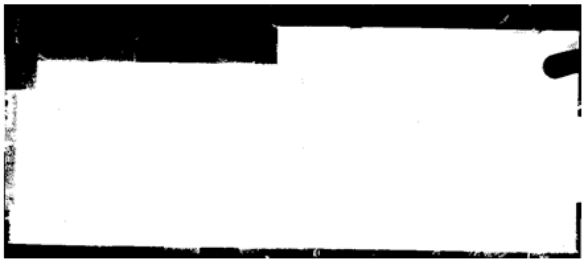

(b) Binary image generated after discretization.

(c) Detected contour (dilated).

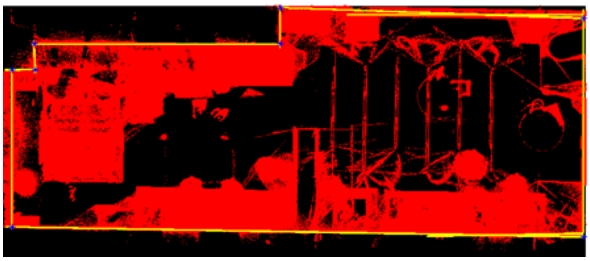

(d) Walls and their intersections recovered by the Hough transform and plane intersection stages.

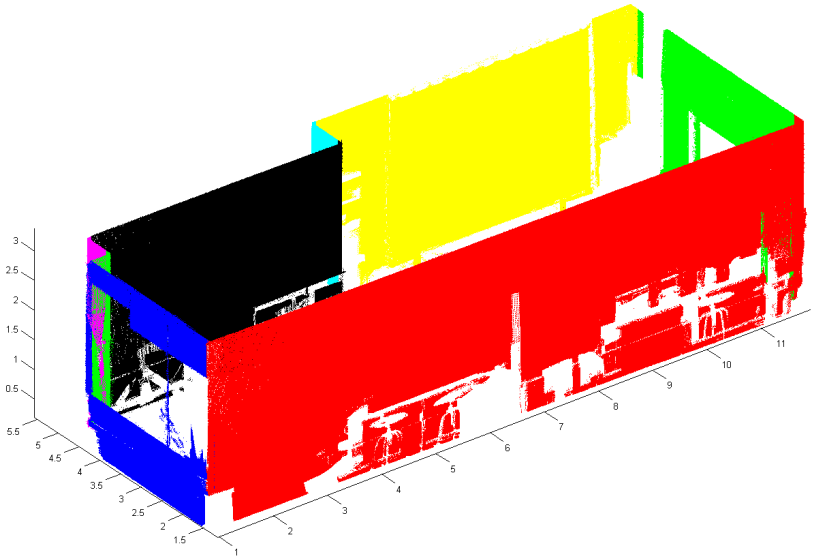

(e) 3D points matched to the detected walls.

FIG. 5. Illustration of the wall segmentation process.

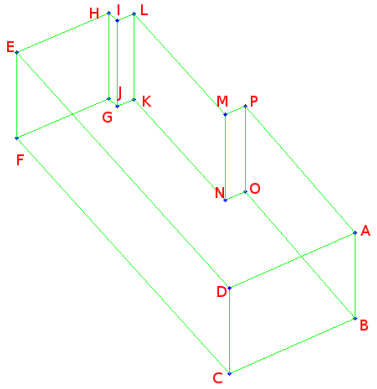

FIG. 6. Reconstructed B-rep of the room structure (boundary elements only) from the segmentation results reported in Figures 4(b) and 5(e).

Once the points belonging to walls, ceiling and floor are removed from the original 3D point cloud, the points corresponding to the top part of the room are extracted. This area, colored in blue in Figure 7(a), is expected not to include other large components but the searched columns. A top view of that point cloud slice is converted into a binary image (see Figure 7(b)) and the connected segments whose bounding boxes are large enough are considered as potential 'free' columns.

For each of those segments, a least-square-error technique is used to fit circles (Kasa 1976) and rectangles (Chaudhuri and Samal 2007) to it. If the fitting is good, the column is considered recognized and is modelled by extruding the detected cross-sections from the floor up to the ceiling of the room (Figure 7(c)).

Modeling of wall openings

A novel approach is proposed to detect and model significant rectangular wall openings such as doorways and windows. The approach, illustrated in Figure 8, is based on the detection of moldings around empty areas (without 3D points) within wall planes.

For each wall plane, the first step consists in generating a 2D binary image I_{wall} discretizing the point cloud data. Each pixel in I_{wall} is labeled occupied or empty, depending on whether at least one 3D point falls within it (green pixels in Figure 8(a)). This yields the detection of the boundary of empty regions (Figure 8(b)) that may correspond to openings (empty regions can also be the result of occlusions).

Next, for each empty region an opening molding is searched by detecting a specific 3D point pattern which is maintained for a set of thin and continuous vertical and horizontal slices along its boundary. Let's assume that a segment P_i which borderlines an empty area of the wall maintains the signature f_1 (see Figure 9). Since f_1 is not a constant function, the segment P_i is a candidate to be a molding location. Candidate molding locations are searched all along the boundary of the opening, classified through a signature matching process detailed in (Valero et al. 2011), and grouped into vertical and horizontal molding segments (see blue and red lines in Figure 8(c)). Finally, doors and windows are detected by means of a region-growing algorithm that finds empty regions bounded by horizontal and vertical molding segments, as shown in Figure 8(d). The region-growing algorithm has two steps. First, a horizontal line sweep detects empty regions bounded by horizontal molding segments. Then, these initial regions are expanded horizontally to vertical

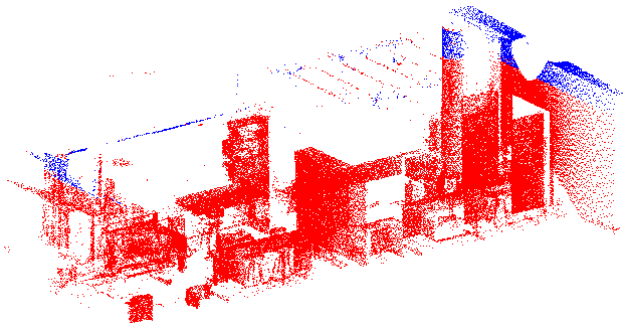

(a) Point cloud D_3 with the extracted top part in blue.

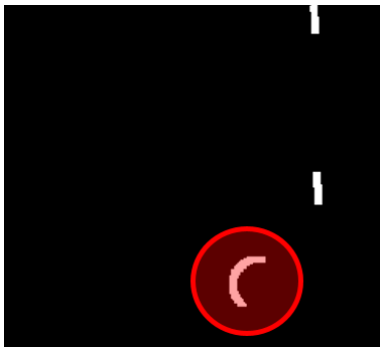

(b) Segment candidates of column cross-sections.

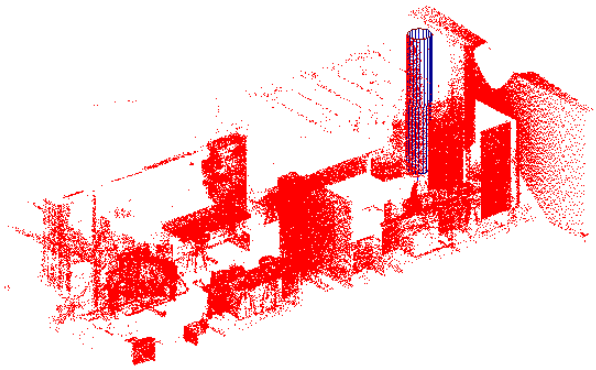

(c) 3D model of the recognized columns.

FIG. 7. Illustration of the process for detecting interior 'free' columns.

molding segments. Regions bounded by an upper and lower segment are classified as windows. Regions that extend to the floor are classified as doors. Note that the process assumes that openings are rectangular and all their sides (three for a door, and four for a window) are at least partially captured during scanning so that molding segments can be detected.

Although this method focuses on the case of openings with moldings, it can also be employed in the case of openings which do not have a molding but are recessed. In such case, the signature simply consists of a step function (see Figure 10).

Final B-Rep model

The detected 'free' columns and openings are easily added to the initial room boundary B-Rep model (Figure 6) using planar surfaces and lines, as well as topological information (faces, edges and points). Figure 11 shows the final B-Rep model obtained for the illustrative interior space.

Modeling of furniture

The furniture in the scene is identified, recognized and positioned with the help of RFID tags attached on them, as well as relevant geometric information contained in the building's FM database. An RFID reader mounted alongside with the scanner acquires the object IDs stored in the tags during the scanning process. Each ID has a corresponding entry in the FM information database that provides relevant relevant geometric information about the given object. These researchers

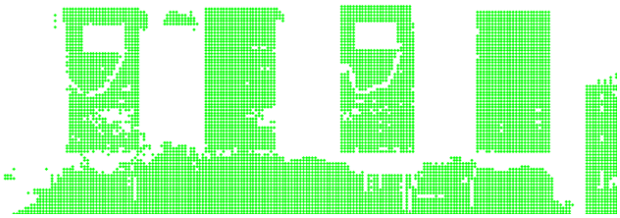

(a) Marked empty areas in a wall plane

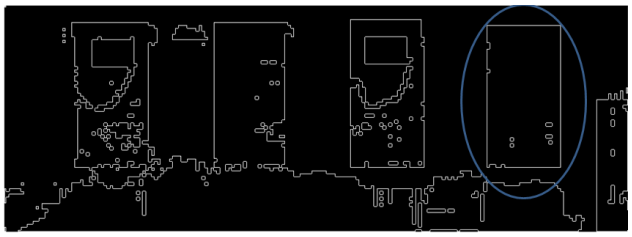

(b) Boundaries of empty areas of a wall and extracted 3D data for one of them.

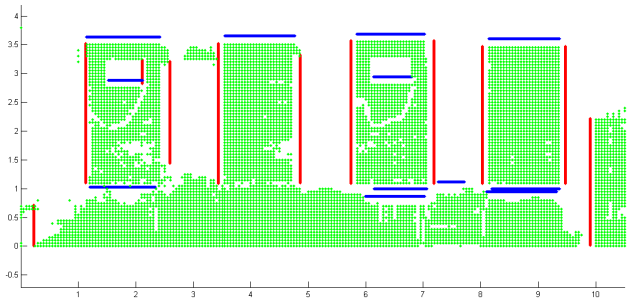

(c) Detection of horizontal and vertical moldings. The vertical moldings are shown in red and horizontal moldings, in blue.

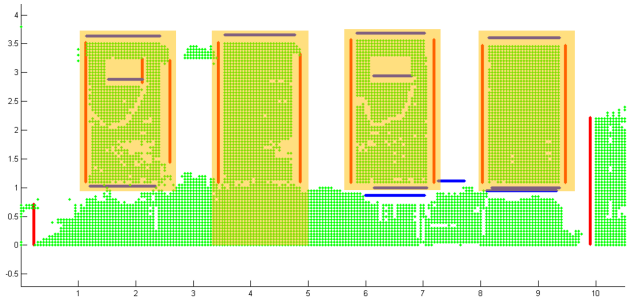

(d) Final detections and modeling of the openings. The figure illustrates three windows and one door correctly detected, and one wrongly detected 'door'-like opening.

FIG. 8. Illustration of the opening detection process.

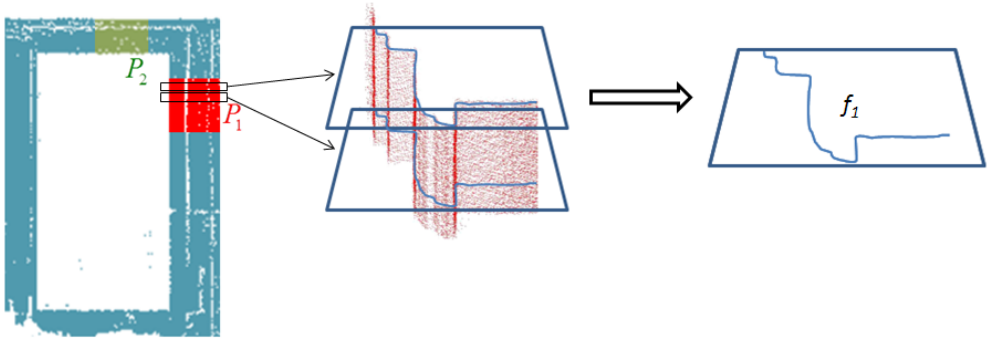

FIG. 9. Function fitting the projected data of a molding.

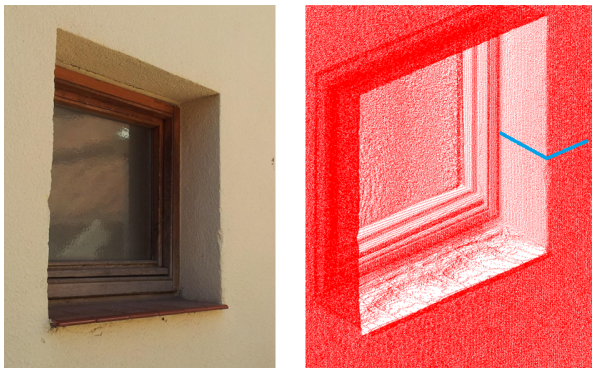

FIG. 10. Opening without a molding. In such case, the recess profile (marked in the figure on the right) can be used with our window detector.

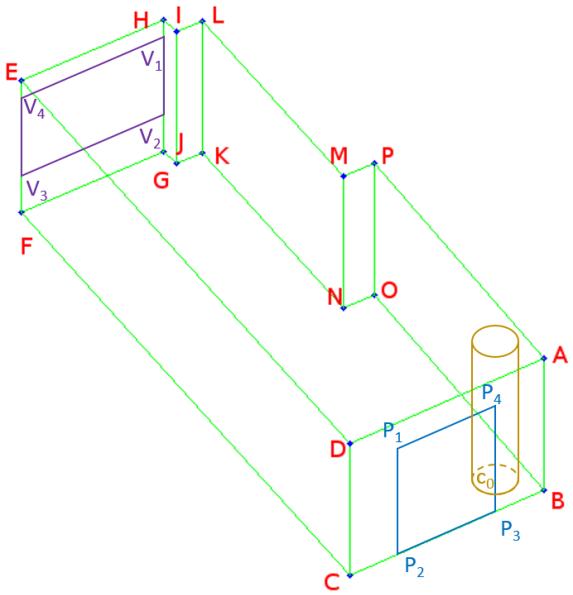

FIG. 11. Final B-Rep model with columns and openings.

particularly store for each object:

- *Discriminatory geometric information*, used to uniquely recognize/locate this object in the point cloud data; and
- *3D model (mesh)*, used to accurately position the object in the point cloud data, and subsequently for visualization.

The following sub-sections present the methods developed to recognize and determine the pose of the following types of furniture: tables, chairs, wardrobes (and the like), and paper baskets. Note that all these elements are assumed to be in contact with the floor in a stable position.

Tables

The discriminatory geometric information used to recognize a table in the point cloud data includes: the length, width and height of the tabletop.

The recognition process, illustrated in Figure 12, goes as follows. A horizontal slice of the current 3D point cloud (D_4) is first extracted at the table height, and a binary image I_t is generated by projecting the points contained in that slide orthogonally onto a horizontal plane, and labelling the pixels of I_t as *occupied* (by points) or *empty*. Compact regions in the image are filtered by calculating the normal vectors of the points by means of an algorithm based on the scatter matrix (Shi et al. 1994) – see Figure 12(d) how the boundary of the tabletop is clearly distinguished. Then, the lengths of the two main orthogonal directions of the compact regions are used as recognition criterion. The main directions also enable the initial approximate positioning of the table's 3D model (from the FM database) in the scene. This position is subsequently optimized by finely fitting the 3D model to the complete point cloud by means of an Iteration Closest Point (ICP) algorithm (Rusinkiewicz and Levoy 2001).

Chairs

The discriminatory geometric information used to recognize a chair in the point cloud data is: the leg pattern to be searched at a specified height above the floor.

The recognition process starts with the extraction of a slice of the point cloud around the specified height above the floor, and the generation of a binary image I_c from the points contained in that slide projected on a horizontal plane. The goal of the subsequent image processing is to recognize the leg pattern, i.e. signature, of the given chair in the image. The authors distinguish discrete from continuous leg patterns. Discrete patterns consist of sets of spots disposed at the vertices of regular polygons (see example in Figure 13(a)), and continuous patterns are continuous patches usually with a star shape (see example in Figure 14(a)).

In the case of *discrete patterns* (Figure 13), since the projections of the legs are discrete, each being only a few centimeters wide, only small and compact segments are considered as potential legs, and their patterns studied. For each possible leg, its distance to the other ones is calculated, and the pattern of these distances is checked against the expected one. For a chair having n legs, any set of n potential legs obeying the chair distance pattern conditions simultaneously is selected as candidate for the considered chair.

In the case of *continuous patterns* (Figure 14), a shape matching process is executed by cross-correlating the leg pattern (calculated beforehand from the chair's 3D model) with image I_c. To address the fact that the orientation of the chair leg pattern in the room is unknown, this process

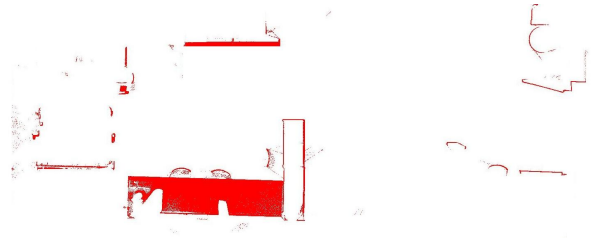

(a) 3D points inside the slice defined around the expected tabletop height.

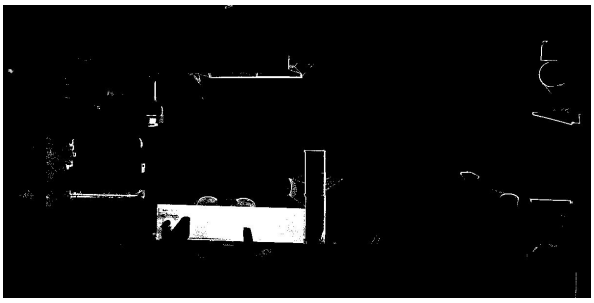

(b) Binary image I_t.

(c) Extracted segment.

(d) Normal vectors for the detected segment.

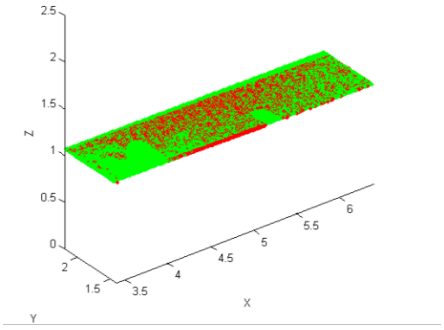

(e) Recognized tabletop (in green) from the segment 3D points (in red).

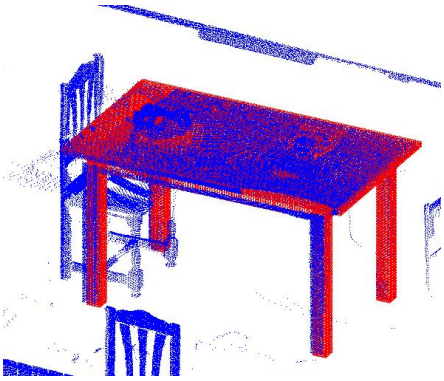

(f) Final positioning of the table (red) in the entire point cloud.

FIG. 12. Illustration of the process to recognize and model a table.

is conducted $\frac{360}{2n}$ times with 2° incremental rotations of the pattern between two consecutive cross-correlation operations.

In both the discrete and continuous cases, the detection stage yields an initial pose of the chair that is refined by using an ICP algorithm to fit the 3D model of the chair to the 3D point cloud data of the scene. To address issues surrounding symmetries in the chair leg layout, the ICP algorithm is also initialized n times.

(a) Example of a discrete pattern.

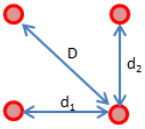

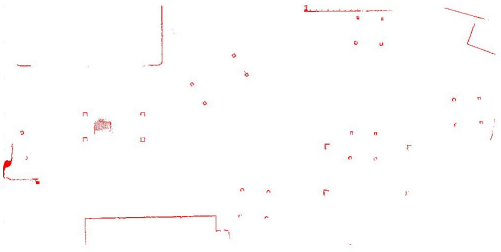

(b) Slice of points close to the floor.

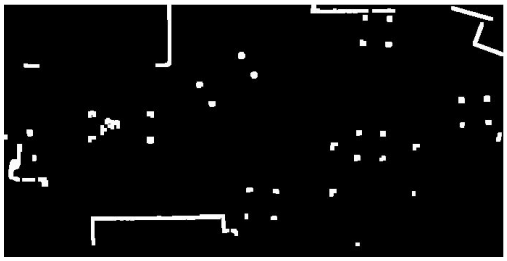

(c) Binary image I_c.

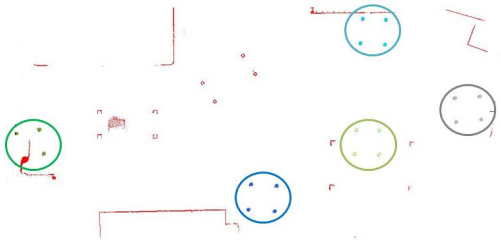

(d) Detection of the discrete pattern (multiple detections).

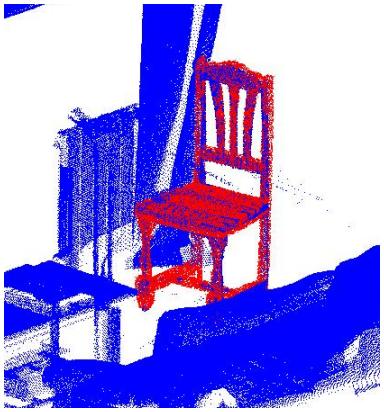

(e) 3D chair model accurately positioned in the scene.

FIG. 13. Illustration of the process for detecting and modeling a chair with a discrete leg pattern.

Wardrobe-like furniture

Wardrobe-like furniture, like wardrobes, filing cabinets, or chest of drawers, are hypothesized to be shaped as parallelepipeds. As a result, the discriminatory geometric information used to recognize a wardrobe-like piece of furniture in the point cloud data is: the width, depth and height of the parallelepiped.

As illustrated in Figure 15, the recognition algorithm is based on processing an image which is obtained from the subtraction of two point cloud data slices, above and below the specified wardrobe height. Two binary images I_{w_1} and I_{w_2} are generated from these slices, and the subtraction binary image $I_w = I_{w_1} - I_{w_2}$ is processed. The wardrobe is detected in I_w as the white

(a) Example of a chair with a continuous leg pattern.

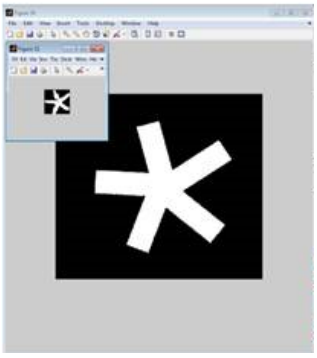

(b) Binary pattern obtained from the chair's 3D model and used for the cross-correlation step.

(c) Binary image of the top view of the point cloud slices (I_c).

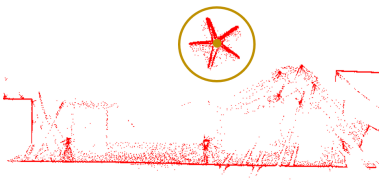

(d) Detection of the continuous pattern.

FIG. 14. Illustration of the process for detecting and modeling a chair with a continuous leg pattern.

segment whose bounding box has the correct width and depth.

The 3D model of the wardrobe (from the database) is then initially positioned by placing its center at the centroid of the point cloud, and aligning the normal vectors of the planes extracted from the matched segment to those of the 3D model. Finally, ICP is employed to adjust the wardrobe's position so that it optimally fits the overall point cloud data.

Paper Baskets

There exist other kinds of furniture such as wastepaper baskets which can also be easily recognized and modelled. Baskets are hypothesized to have a constant cylindrical or rectangular cross-section with vertical longitudinal axes. Therefore, the discriminatory geometric information used to recognize a wastepaper basket in the data is: its cross-section type and size, and its height.

The approach to detect and model these objects is similar to the one used for interior structural columns, that is the detection of the cross-section in a binary image obtained from a horizontal slice of the point cloud data spanning from the floor to the specified basket height. Like for other furniture, the initial position yielded by this process is refined using ICP. Figure 16 shows two wastepaper baskets recognized and modelled in a scene.

EXPERIMENTAL RESULTS

The proposed system has been tested with diverse real inhabited interiors. These researchers first present results for what can be considered a 'simple' case of a living room. Then, results for

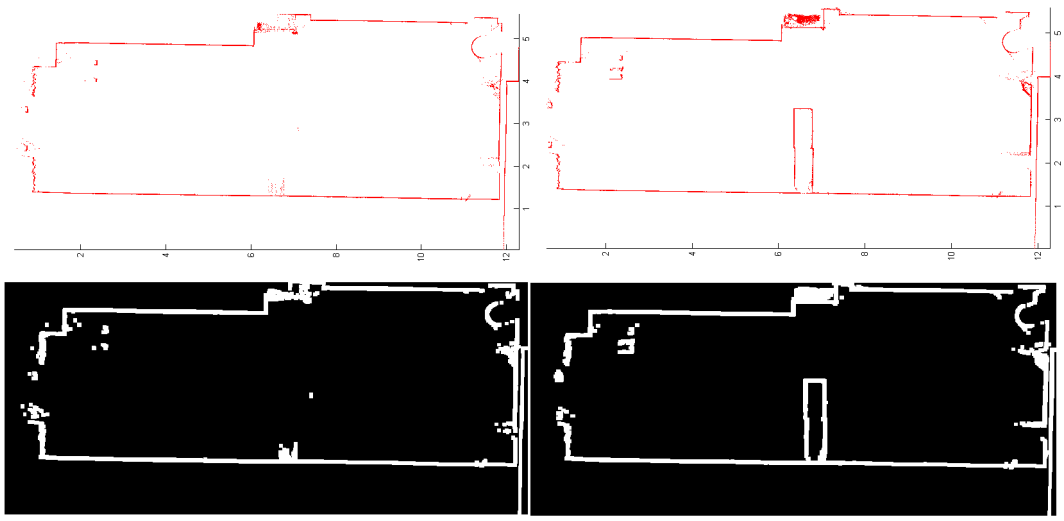

(a) Slices above and below the wardrobe height (first row) and respective binary images I_{w_1} and I_{w_2} (second row).

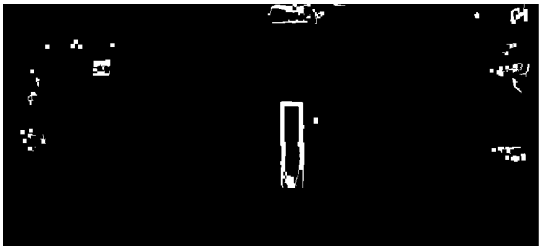

(b) Subtraction image I_w.

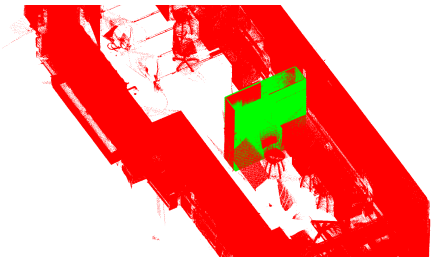

(c) Final position of the wardrobe model superimposed to the point cloud.

FIG. 15. Wardrobe-like furniture detection and positioning.

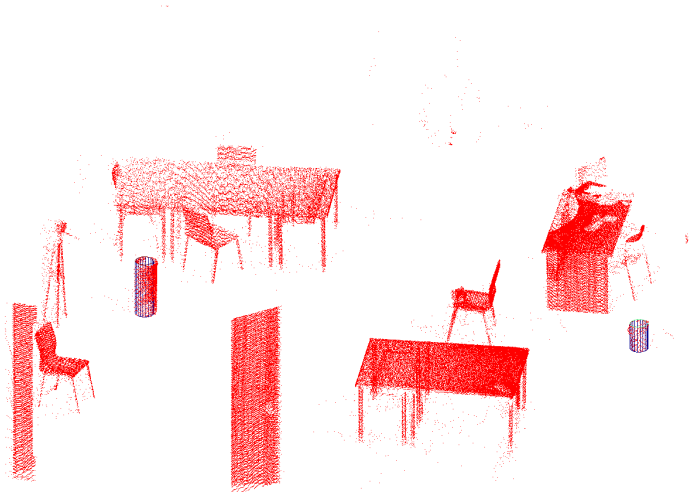

FIG. 16. Example detection and modeling of two wastepaper baskets.

a more 'complex' case of an entire high-school floor are reported. Altogether, these results enable a fair assessment of the current performance of the system.

A simple case: A living room

The approach has first been tested in the context of a living room, for which three different furniture configurations have been arranged are scanned. The experimental equipment setup is composed of a Faro Photon 80 laser scanner and an OBID LRU 3500 (FEIG) RFID sensor. The sensor platform is moved towards commanded positions to perform scans. For each room configuration, 3D data was acquired from five positions, resulting in a total of eight million points. Figure 17 presents the plan of the room and Table 1 summarizes the number of tagged furniture in each configuration.

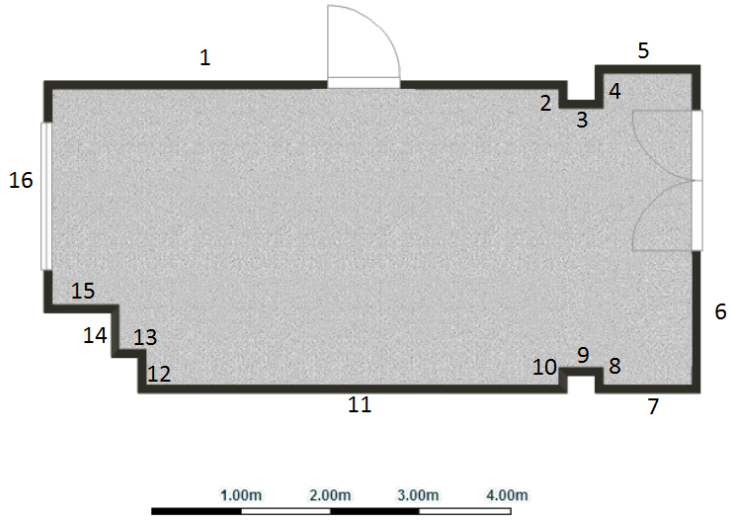

FIG. 17. Plan of the living room.

Room configuration	I	II	III
Tables	3	3	3
Chairs	5	6	5
Wardrobes	2	2	3

TABLE 1. Number of tagged furniture for each of the three room configurations.

Structure

Once the 3D data are acquired and aligned, and the floor, ceiling and walls are recognized and modelled, the precision of the obtained B-Rep models is assessed. The distances between points and planes are represented in color maps in Figure 18. Note that regions corresponding to objects like pictures or moldings are clearly visible through significant color variations. For example, two paintings and the skirting board, whose width is between 1 and 1.5 cm, can be seen in Wall 7 (Figure 18(b)). Of course, some of error is also due to walls not being totally flat.

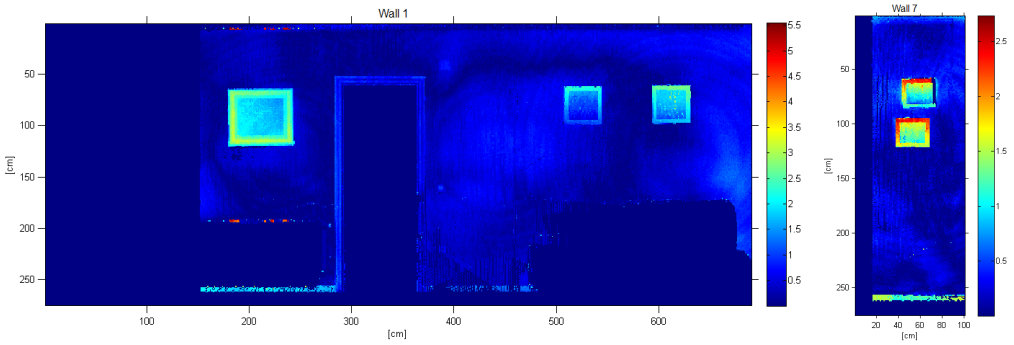

(a) Wall 1. (b) Wall 7.

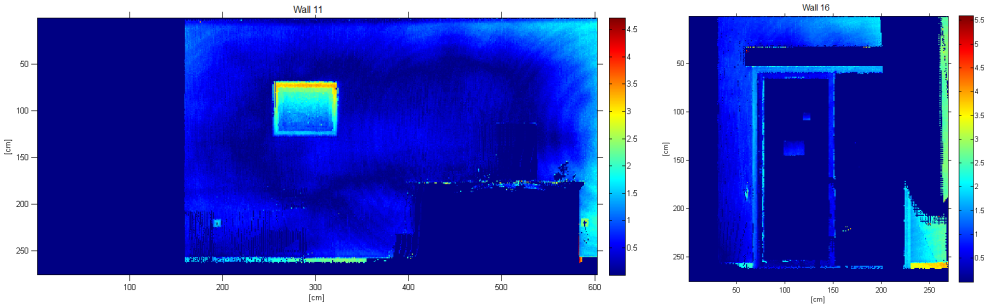

(c) Wall 11. (d) Wall 16.

FIG. 18. Error maps obtained after the plane fitting stage, for four representative walls. The error is simply the distance (cm) of each point to the fitted plane.

The precision of the wall detection and modelling is also assessed with the following four quantitative metrics. The latter three are obtained by comparing the generated B-Rep model to a *ground-truth* model previously built manually using measurements obtained with a Leica DISTO^{TM} A6 laser distance meter.

- δ: the plane fitting error, i.e. the mean value of the distances of the matched points to the calculated wall plane.
- α: the plane orientation error, i.e. the horizontal angle between the ground-truth and estimated normal vectors.
- d_h and d_w: the wall height and width errors, i.e. the differences between the ground-truth and estimated heights and widths.

Table 2 summarizes the results obtained for all 16 walls. The values of δ range from 0.2 to 1.6 cm, demonstrating good modelling precision. Note that values above 1 cm are generally obtained for narrow walls only. The values of α do not exceed 1.6°, with errors above 1° typically obtained for narrow walls. The values for d_h are all 0.80 cm. This is simply due to the fact that d_h effectively assesses the accuracy in the modelling of the floor and ceiling that are both considered to be flat horizontal surfaces. The values for d_w range between 0.1 and 4.5 cm, with errors above 2 cm are essentially obtained for narrow walls.

Altogether, the results are very positive. The accuracy of the modelling is generally high, with larger errors only noticed for narrow walls. Wall 16 may first be considered an exception to

441 this. But, as shown in Figure 18(d), the presence of a large window and the additional significant
442 occlusion from curtains on one of its side do explain the comparatively poorer results.

Wall ID	δ [cm]	α [°]	d_h [cm]	d_w [cm]
1	0.65	0.23	0.80	0.74
2	1.15	1.83	0.79	0.39
3	0.35	0.32	0.79	0.09
4	0.54	1.42	0.80	0.99
5	0.87	0.21	0.79	0.15
6	1.00	0.06	0.79	1.80
7	0.49	0.87	0.80	0.11
8	1.32	0.02	0.80	2.05
9	0.33	0.12	0.80	0.32
10	1.19	2.33	0.80	1.46
11	0.63	1.21	0.80	2.18
12	1.07	2.04	0.80	1.31
13	0.65	0.54	0.80	1.29
14	0.99	0.53	0.80	2.15
15	0.50	0.42	0.80	1.17
16	1.63	0.20	0.80	4.45
Mean	0.84	0.77	0.80	1.29

TABLE 2. Modelling errors for each room wall. δ is the plane fitting error. α is the plane orientation error, i.e. the horizontal angle between the measured ground-truth and estimated normal vectors. d_h and d_w are the plane dimensional errors (absolute value), i.e. the differences between measured ground-truth and estimated heights and widths.

443 As shown in Figure 19, three openings corresponding to two open doors and one window are
444 detected. The figure also shows their estimated sizes and positions. To quantitatively evaluate the
445 accuracy of the detection and modeling of these components, three metrics are used:

446 • d_c: the positioning error, i.e. the distance between the centers of the reconstructed and
447 ground-truth opening models; and
448 • d_h and d_w: the sizing errors, i.e. the differences in the, respectively, height and width of the
449 reconstructed and ground-truth opening models.

450 The results, summarized in Table 3, show that the doors fit better than the window. For the window,
451 the error is due to curtains that partially occlude it, leading to the fitting of the component to a
452 smaller opening.

453 *Furniture*

454 Figure 20 illustrates the three furniture configurations arranged for the living room, and the re-
455 construction results. Different pieces of furniture are identified and positioned in each point cloud.

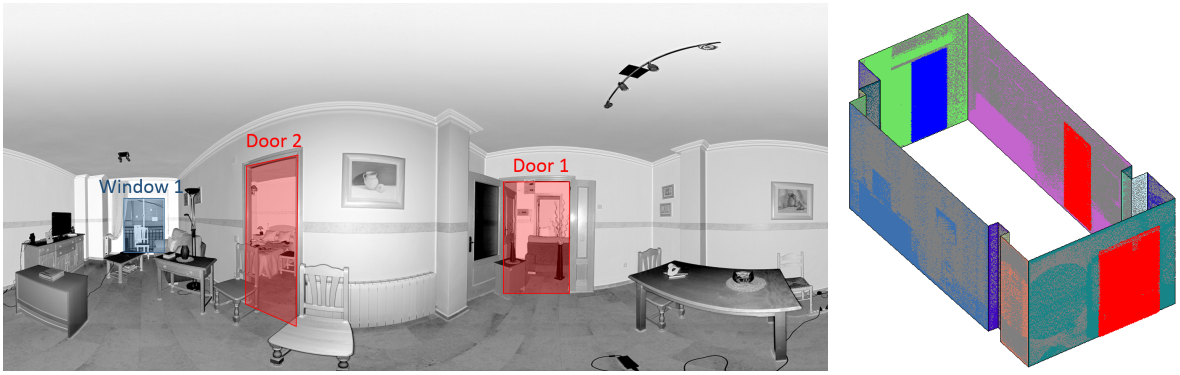

(a) Planar image of the room with the detected and modeled openings.

(b) B-Rep model with the detected openings.

FIG. 19. Result of the detection and modelling of openings.

Opening	d_c [cm]	d_h [cm]	d_w [cm]
Door 1	0.78	0	2
Door 2	1.07	0	1
Window	41.76	2	87

TABLE 3. Calculated parameters for the identified openings in the living room.

Several components such as curtains, a sofa and other small objects are correctly not recognized in this process.

To evaluate the recognition and positioning results, ground truth models for all configurations were generated in advance. The 3D model of each piece of furniture is stored in the FM database as a regular triangular mesh with a density of 1 vertex per $5mm^2$. This mesh resolution is selected to be similar to the points density of the room point cloud, in order to ensure that the ICP-based fine positioning algorithm performs appropriately (see section 4). Note that the mesh resolution could be adapted automatically to the point density of the point cloud.

The performance of the recognition and positioning of the furniture is assessed quantitatively using the metrics below. The first two are based on the distances between corresponding vertices in the mesh models positioned in the ground-truth and recognized and modelled positions:

- d: the average distance (cm) between corresponding points.
- P: the percentage of corresponding points that are closer than a threshold distance; 2.5 cm is used.
- $\mathbf{T} = \{\mathbf{R}, \mathbf{t}\}$: the rigid transformation error, i.e. the transformation matrix $\mathbf{T}$, with rotation $\mathbf{R}$ and translation $\mathbf{t}$, required to align the reconstructed model to the ground-truth model. This error can be decomposed into the rotational error, for example with the Euler angles (α, ϕ, θ) or the quaternion angle μ, and the translation error with the translation vector components $\mathbf{t} = [x, y, z]^\mathsf{T}$.

Table 4 summarizes the results for each piece of furniture, and overall. As can be seen, all

(a)

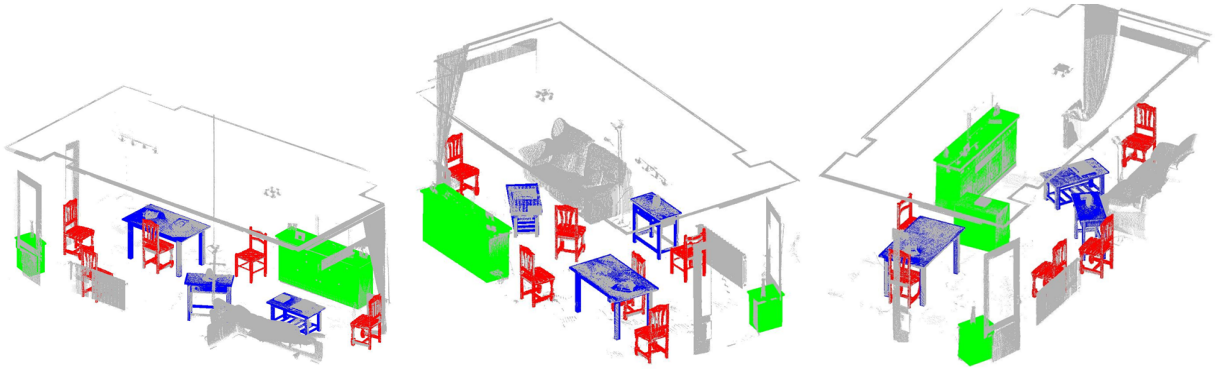

(b)

FIG. 20. Furniture recognition and modeling results for the three different configurations. Configurations I, II and III are shown in the three successive columns. a) Planar views of the acquired point cloud data. b) Recognized and positioned furniture.

objects are accurately recognized and precisely positioned The values of d are below 1.5 cm and P above 85%. Angular errors oscillate between 0 and 1°, and location (i.e. translation) errors are below 2 cm in most cases. The exception of Wardrobe 2 is noticeable (although the error is most of the time not that significant). The reason for the poorer results obtained for Wardrobe 2 is that, in all configurations, it is positioned in the corner of the room, which results in insufficient data being acquired for precise positioning. Also, its width and depth are very similar, which can lead to a 90° rotation error around the vertical axis, as can be seen in Configuration II.

The complete 3D models generated for the three configurations are shown in Figure 21. These models are created by means of solid modeling software using the calculated B-Rep for the room structure, the furniture mesh models and their calculated poses.

A more complex case: The first floor of a high school

This sub-section presents the results obtained for the first floor of a high school composed of five rooms and one corridor and equipped with typical classroom furniture. The experimental equipment setup is composed of a mobile robot equipped with a Riegl VZ-400 laser scanner, an OBID LRU 3500 (FEIG) RFID sensor, and two computers (see Figure 22). The mobile robot is able to move towards commanded positions to perform scans.

In total, 30 scans were acquired and 6 floors, 6 ceilings, 94 walls, 5 doors, 15 windows, 33 chairs, 15 tables and 4 wastepaper baskets are recognized and modelled. Figure 23 shows the complete point cloud for the floor.

In order to evaluate the performance of the method, a *ground truth* model of the scenario and a database containing over 200 3D models of pieces of furniture were created. As in the living-room

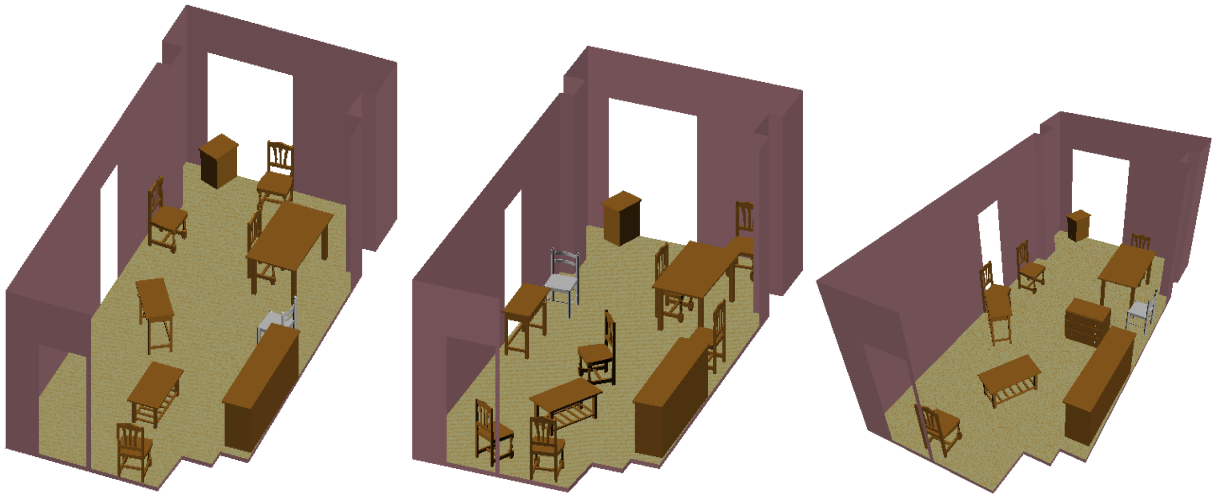

FIG. 21. 3D furnished models for the three configurations of the studied living room. Part of the B-Rep has been cropped for visualization purpose.

FIG. 22. Experimental equipment setup on board the mobile robot.

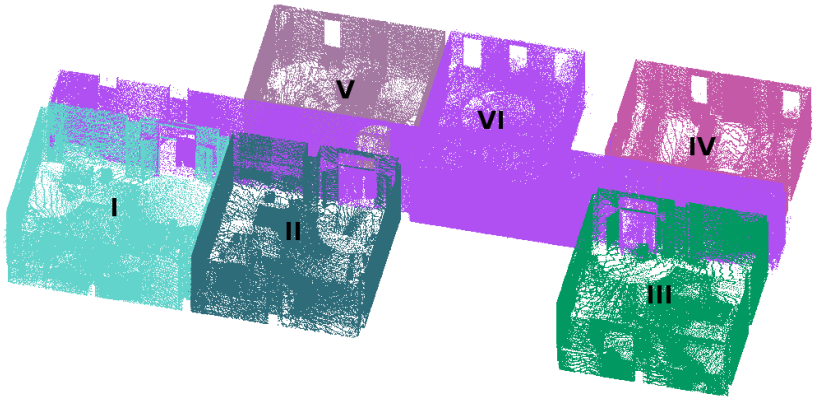

FIG. 23. Point cloud of the first floor of a high school.

Conf.	Obj.	$d[cm]$	$P[\%]$	$\alpha[^\circ]$	$\phi[^\circ]$	$\theta[^\circ]$	$\mu[^\circ]$	$x[cm]$	$y[cm]$	$z[cm]$	$\|\mathbf{t}\|\,[cm]$
I	**C1**	1.28	88.40	0.04	0.25	0.80	**0.82**	0.80	1.01	0.81	**0.87**
	C2	1.63	80.74	0.50	0.43	0.86	**1.08**	1.03	0.19	2.99	**1.40**
	C3	1.82	80.10	0.15	0.32	0.52	**0.62**	0.59	1.61	3.30	**1.83**
	C4	1.69	100	0.38	0.01	0.22	**0.44**	1.03	0.65	1.35	**1.01**
	C5	1.68	99.47	0.28	0.60	0.22	**0.7**	0.80	0.50	1.59	**0.96**
	W1	1.83	81.61	0.76	0.86	0.12	**1.16**	1.02	2.21	2.75	**1.99**
	W2	1.84	53.43	1.78	1.95	2.67	**3.78**	3.88	5.00	2.18	**3.69**
	T1	0.84	100	0.00	0.00	0.16	**0.16**	1.11	0.63	0.83	**0.86**
	T2	1.06	99.98	0.06	0.06	0.89	**0.9**	0.09	0.85	1.71	**0.88**
	T3	0.30	100	0.05	0.00	0.05	**0.06**	0.17	0.41	0.05	**0.21**
II	**C1**	1.58	99.08	0.63	0.49	0.64	**1.02**	1.00	0.34	1.22	**0.85**
	C2	1.72	99.25	0.69	0.14	1.40	**1.56**	0.39	1.63	0.96	**0.99**
	C3	0.99	96.13	0.18	0.02	0.90	**0.92**	0.52	0.41	0.58	**0.50**
	C4	1.73	98.31	0.48	0.56	1.03	**1.26**	0.96	1.21	1.26	**1.14**
	C5	1.88	92.67	0.34	1.32	0.28	**1.38**	1.63	1.78	1.52	**1.64**
	C6	1.75	73.4	1.23	0.15	1.15	**1.7**	0.48	2.89	1.11	**1.49**
	W1	1.67	66.08	0.87	0.87	0.41	**1.3**	1.57	1.40	4.41	**2.46**
	W2	1.75	51.88	0.04	2.3	105.99	**106**	8.64	1.17	1.58	**3.80**
	T1	0.93	99.65	0.01	0.01	1.23	**1.24**	1.15	0.45	1.00	**0.87**
	T2	1.45	86.98	0.02	1.34	0.52	**1.44**	1.97	2.14	2.06	**2.06**
	T3	0.89	69.55	0.23	0.03	2.03	**2.04**	2.89	9.54	0.74	**4.39**
III	**C1**	1.73	97.16	0.56	0.54	0.79	**1.1**	0.33	1.80	1.41	**1.04**
	C2	1.54	100	0.13	0.23	0.81	**0.86**	0.55	0.27	1.21	**0.68**
	C3	1.67	82.95	0.27	0.15	0.03	**0.32**	1.00	0.11	1.48	**0.86**
	C4	1.84	93.76	0.20	0.83	0.61	**1.06**	1.86	0.18	1.37	**1.14**
	C5	1.41	83.21	0.16	0.35	0.78	**0.88**	1.19	1.15	0.82	**3.16**
	W1	1.66	77.61	0.57	0.83	0.03	**1**	1.14	1.29	3.67	**2.03**
	W2	1.58	71.68	4.61	1.07	0.88	**4.82**	0.85	0.64	3.87	**1.79**
	W3	1.68	100	0.21	0.10	0.09	**0.24**	1.74	0.61	1.17	**1.17**
	T1	0.91	100	0.03	0.00	0.37	**0.38**	1.63	0.36	0.96	**0.98**
	T2	1.22	90.57	0.00	0.08	0.51	**0.52**	2.64	0.95	1.70	**1.76**
	T3	0.72	87.48	0.06	0.22	0.99	**1.02**	3.28	0.85	0.44	**1.52**
	Mean	**1.45**	**87.54**	**0.49**	**0.50**	**3.99**	**4.43**	**1.50**	**1.38**	**1.63**	**1.56**

TABLE 4. Furniture recognition and positioning results for the three configurations (C $\rightarrow$ chair, W $\rightarrow$ wardrobe; T $\rightarrow$ table). μ is the quaternion angle of the rotational error.

example, the evaluation of the performance is carried out considering different quantitative metrics assessing the accuracy of the B-Rep model, and furniture recognition and modeling accuracy and precision.

Structure

The accuracy of the B-Rep model is evaluated using the following metrics that assess performance per room (as opposed to per component):

- Walls:
  - $\bar{\alpha}$: mean error (per room) in the wall horizontal orientation.
  - $\bar{d_h}$ and $\bar{d_w}$: mean error (per room) in the height and width of the walls.
- Openings
  - $\bar{d_c}$: mean error (per room) in the positioning within the wall plane of the centres of the openings.
  - $\bar{d_h}$ and $\bar{d_w}$: mean error (per room) in the height and width of the openings.

Table 5 summarizes the results. Overall, walls are well fitted, with $\bar{\alpha}$ well below 2° for all rooms. Regarding the width of the walls, errors range from 1 cm to 6 cm, with average relative error of 2.3%. Regarding the height of the walls, errors are extremely small, $\ll 1$ cm, which demonstrates the precision of the ceiling and floor detection and plane fitting process.

Table 6 summarizes the recognition and modelling precision for the openings. Although similar results are generally obtained for both kinds of openings, a lower precision can be noticed for windows. This is due to the presence of blinds that partially occlude the top parts of some windows, resulting in the windows' geometries not being accurately calculated.

The final B-Rep model containing floors, ceilings, walls and openings for all the rooms is shown in Figure 24.

Room	$\bar{\alpha}$ [$^\circ$]	$\bar{d_h}$ [cm]	$\bar{d_w}$ [cm]
I	1.47	<0.01	2.28
II	0.64	0.02	3.78
III	0.54	<0.01	5.05
IV	1.07	0.01	6.03
V	0.10	0	0.86
VI	0.73	0.04	4.94

TABLE 5. Reconstruction performance for the walls, ceilings and floors. $\bar{\alpha}$ is the mean error in the walls' horizontal orientations; $\bar{d_h}$ and $\bar{d_w}$ are the mean errors in the heights and widths of the walls.

Opening	$\bar{d_c}$ [cm]	$\bar{d_h}$ [cm]	$\bar{d_w}$ [cm]
Doors	3.14	0.8	4.92
Windows	3.75	4.98	4.08

TABLE 6. Reconstruction performance for doors and windows (openings).

Furniture

The performance of the recognition and positioning of furniture is assessed per room using the following quantitative metrics, relating to those used earlier:

- $\bar{d}$, the mean of the d values obtained for all furniture contained within the given room.
- $\bar{P}$, the mean of the P values obtained for all furniture contained within the given room.

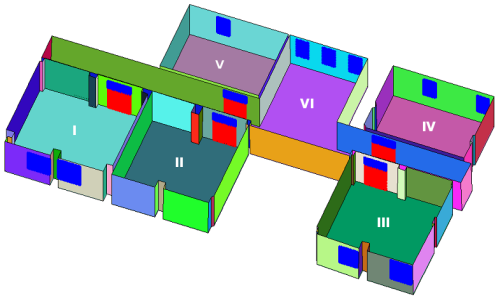

FIG. 24. B-Rep model obtained (red → doors; blue → windows).

- $\bar{\mu}$: the mean of the quaternion angular errors obtained for all furniture contained within the given room.
- $\|\bar{t}\|$: the mean of the position error obtained for all furniture contained within the given room.

Table 7 summarizes the results obtained by the proposed approach. All $\bar{P}$ values are again higher than 70% and $\bar{d}$ values are below 2 cm, which indicates that all objects have been correctly recognized. Accordingly, low values are accordingly reported for the positioning of the furniture, with $\bar{\mu}$ below 3° and $\bar{t}$ below 2 cm in most cases.

Room	$\bar{d}$ [cm]	$\bar{P}$ [%]	$\bar{\mu}[^\circ]$	$\|\bar{t}\|$ [cm]
I	1.91	78.7	2.87	3.43
II	1.81	78.3	2.56	1.95
III	1.86	78.7	2.82	1.73
IV	1.94	72.8	2.40	1.77
V	1.58	90.9	2.34	1.74
VI	n/a	n/a	n/a	n/a

TABLE 7. Performance of the recognition and positioning of the furniture. $\bar{d}$ and $\bar{P}$ are the averages of the d and P values obtained for all furniture contained within each room. $\bar{\mu}$ and $\bar{t}$ are the means of the orientation and position errors obtained for all furniture contained within the given room. Room VI did not contain any furniture.

Figure 25 shows the complete 3D models (structure + furniture) reconstructed for the rooms II and IV of the high school floor.

CONCLUSIONS

Over the last five years, various partial solutions for automatically generating 3D models of buildings using laser scanners have been published. In the case of inhabited, furnished interiors, the automatic generation of 3D models is considered challenging because of the large amount of information that needs to be processed, the wide variability in room shape and unpredictable furniture layout, and the frequent presence of significant clutter and occlusion.

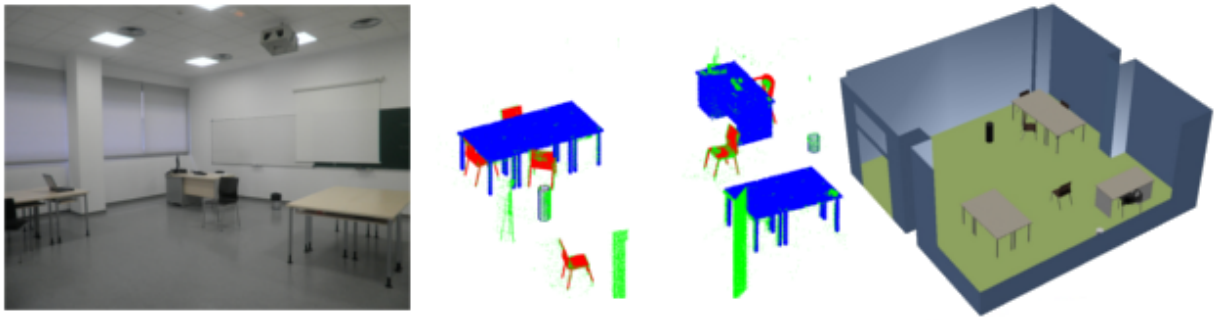

(a)

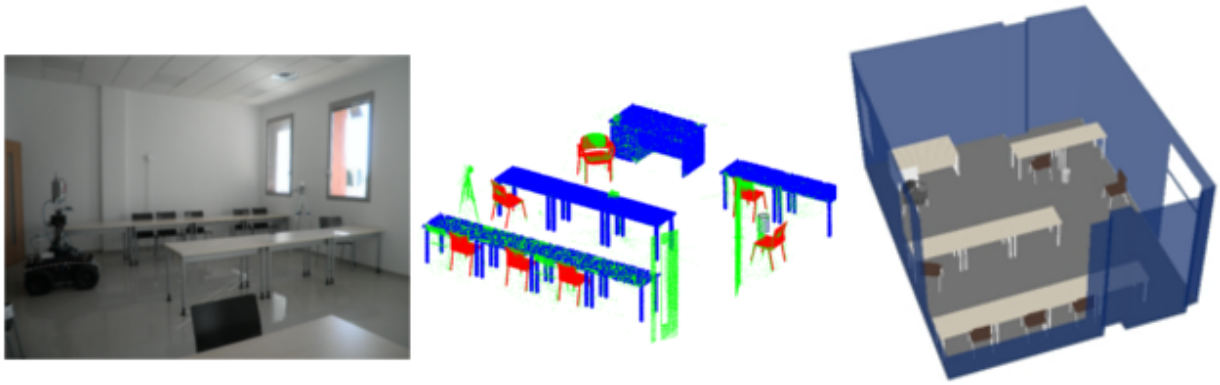

(b)

FIG. 25. Final modeling results for the rooms II (a) and IV (b) of the high-school floor experiment.

This paper proposes a hierarchical 3D data processing algorithm that is able, with the help of RFID technology, to generate detailed and precise semantic 3D models of furnished, inhabited interiors. RFID tags, attached to furniture and scanned at the same time as laser scanning, provide access to discriminatory geometric information (contained in the building's FM database) about the furniture present in the scanned room that greatly alleviates the difficulties of recognizing them in the point cloud data. This makes automatic modeling process more robust, accurate and faster.

Altogether, the approach proposed in this paper is capable of recognizing and modeling the main structural components of an indoor environment (walls, floors, ceilings), the wall openings like doorways and windows, as well as typical furniture, such as tables, chairs and wardrobes. The main contributions reported in this paper over those previously reported in (Valero et al. 2012a; Valero et al. 2012b) are:

1. An improved algorithm is proposed that models wall planes more accurately.
2. B-Rep models of room structures are completed with wall openings, such as windows and doorways, and interior 'free' columns. In particular, a novel algorithm is presented for the recognition of openings based on molding detection.
3. The algorithms for recognizing and calculating the pose of furniture in the point cloud are improved and detailed.
4. Regarding the validation of the system, experimentation is extended to larger environments,

and new assessment procedures are included that further demonstrate the strengths of the method.

Future improvements to the method should be considered in various lines of inquiries. Firstly, the efficiency and robustness of the current system needs to be tested through complex scenarios, including with the additional presence of Mechanical, Electrical, Plumbing and Fire Protection (MEP/FP) components. This will likely result in the need to investigate new detection and segmentation approaches. Next, the structural modelling approach should be extended to detect and model non-planar walls (by design). Secondly, the system currently enables the recognition of rather simple, standard pieces of furniture; future work should consider the recognition of other pieces like sofas, lamps, and pictures. Thirdly, the generation of the discriminative geometric information required to detect the furniture in the 3D point cloud data is currently done manually. But, this process could be conducted automatically given the known object type. Finally, our current opening detection and modeling algorithm is particularly sensitive to occlusions, and should be revisited. As in (Xiong et al. 2013), our idea is to establish an inference algorithm to precisely delimit opening boundaries on the wall.

APPENDIX I. REFERENCES

Adán, A. and Huber, D. (2011). "3D reconstruction of interior wall surfaces under occlusion and clutter." *2011 International Conference on 3D Imaging, Modeling, Processing, Visualization and Transmission (3DIMPVT)*, 275 –281.

Ali, H., Ahmed, B., and Paar, G. (2008). "Robust window detection from 3D laser scanner data." *CISP '08: Proceedings of the 2008 Congress on Image and Signal Processing, Vol. 2*, Washington, DC, USA, IEEE Computer Society, 115–118.

Anil, E. B., Tang, P., Akinci, B., and Huber, D. (2013). "Deviation analysis method for the assessment of the quality of the as-is building information models generated from point cloud data." *Automation in Construction*, 35(0), 507 – 516.

Bohm, J. (2008). "Facade detail from incomplete range data." *The International Archives of the Photogrammetry, Remote Sensing and Spatial Information Sciences*, 653–658.

Bosché, F. (2010). "Automated recognition of 3D cad model objects and calculation of as-built dimensions for dimensional compliance control in construction." *Elsevier Journal of Advanced Engineering Informatics*, 4(2), 55–59.

Budroni, A. and Bohm, J. (2005). "Toward automatic reconstruction of interiors from laser data." *Proceedings of 3D-ARCH*.

Castellani, U., Livatino, S., and Fisher, R. B. (2002). "Improving environment modelling by edge occlusion surface completion." *International Symposium on 3D Data Processing Visualization and Transmission*.

Cerrada, C., Salamanca, S., Adán, A., Perez, E., Cerrada, J. A., and Abad, I. (2009). "Improved method for object recognition in complex scenes by fusioning 3-D information and RFID technology." *IEEE Transactions on Instrumentation and Measurement*, 58, 3473–3480.

Chaudhuri, D. and Samal, A. (2007). "A simple method for fitting of bounding rectangle to closed regions." *Pattern Recognition*, 40, 1981–1989.

Dell Acqua, F. and Fisher, R. (2002). "Reconstruction of planar surfaces behind occlusions in range images." *IEEE Transactions on Pattern Analysis and Machine Intelligence*, 24(4), 569 –575.

Deutsches Institut fur Normung (2005). "Tolerances in building construction - buildings, DIN 18202:2005-10." DIN Deutsches Institut fur Normung.

Dimitrov, A. and Golparvar-Fard, M. (2015). "Segmentation of building point cloud models including detailed architectural/structural features and mep systems." *Automation in Construction*, 51, 32–45.

Ehrenberg, I., Floerkemeier, C., and Sarma, S. (2007). "Inventory management with an rfid-equipped mobile robot." *Automation Science and Engineering, 2007. CASE 2007. IEEE International Conference on*, 1020–1026 (Sept).

El-Hakim, S., Boulanger, P., Blais, F., and Beraldin, J. (1997). "A system for indoor 3-D mapping and virtual environments." *SPIE Proceedings: Videometrics V*, Vol. 3174, San Diego, California.

El-Omari, S. and Moselhi, O. (2011). "Integrating automated data acquisition technologies for progress reporting of construction projects." *Automation in Construction*, 15:3, 292–302.

Fischler, M. A. and Bolles, R. C. (1981). "Random sample consensus: A paradigm for model fitting with applications to image analysis and automated cartography." *Communications of the ACM*, 24(6), 381–395.

Frueh, C., Jain, S., and Zakhor, A. (2005). "Data processing algorithms for generating textured 3D building facade meshes from laser scans and camera images." *Int. J. Comput. Vision*, 61(2),

159–184.
Guo, R. and Hoiem, D. (2013). "Support surface prediction in indoor scenes." *IEEE International Conference on Computer Vision (ICCV), 2013*, 2144–2151 (Dec).
Hahnel, D., Burgard, W., and Thrun, S. (2003). "Learning compact 3D models of indoor and outdoor environments with a mobile robot." *Robotics and Autonomous Systems*, 1, 15–27.
Ishida, H., Tanaka, H., Taniguchi, H., and Moriizumi, T. (2004). "Mobile robot navigation using vision and olfaction to search for a gas/odor source." *Intelligent Robots and Systems, 2004. (IROS 2004). Proceedings. 2004 IEEE/RSJ International Conference on*, Vol. 1, 313–318 vol.1 (Sept).
Jaselskis, E. J., Anderson, M. R., Jahren, C. T., Rodriguez, Y., and Njos, S. (1995). "Radio-frequency identification applications in construction industry." *Journal of Construction Engineering and Management*, 121:2, 189–196.
Jia, Z., Gallagher, A., Saxena, A., and Chen, T. (2013). "3d-based reasoning with blocks, support, and stability." *Computer Vision and Pattern Recognition (CVPR), 2013 IEEE Conference on*, 1–8 (June).
Kasa, I. (1976). "A circle fitting procedure and its error analysis." *IEEE Transactions on Instrumentation and Measurement*, 25, 8–14.
Kim, C., Son, H., and Kim, C. (2013). "Automated construction progress measurement using a 4D building information model and 3D data." *Automation in Construction*, 31, 75–82.
Kwon, S.-W., Bosché, F., Kim, C., Haas, C. T., and Liapi, K. A. (2004). "Fitting range data to primitives for rapid local 3D modeling using sparse range point clouds." *Automation in Construction*, 13(1), 67 – 81.
Lu, W., Huang, G. Q., and Li, H. (2011). "Scenarios for applying RFID technology in construction project management." *Automation in Construction*, 20, 101–106.
Marques, L., Nunes, U., and de Almeida, A. T. (2002). "Olfaction-based mobile robot navigation." *Thin Solid Films*, 418(1), 51 – 58 Proceedings from the International School on Gas Sensors in conjunction with the 3rd European School of the NOSE Network.
Mast, M., Burmester, M., Krger, K., Fatikow, S., Arbeiter, G., Graf, B., Kronreif, G., Pigini, L., Facal, D., and Qiu, R. (2012). "User-centered design of a dynamic-autonomy remote interaction concept for manipulation-capable robots to assist elderly people in the home." *Journal of Human-robot interaction*, 1(1), 96–118.
Mortenson, M. (1985). *Geometric Modeling*. John Wiley and Sons.
Okorn, B., Xiong, X., Akinci, B., and Huber, D. (2010). "Toward automated modeling of floor plans." *Proceedings of the Symposium on 3D Data Processing, Visualization and Transmission*.
Pu, S. and Vosselman, G. (2009). "Knowledge based reconstruction of building models from terrestrial laser scanning data." *ISPRS Journal of Photogrammetry and Remote Sensing*, 64(6), 575 – 584.
Remondino, F., El-Hakim, S., Girardi, S., Rizzi, A., Benedetti, S., and Gonzo, L. (2009). "3D virtual reconstruction and visualization of complex architectures." *Proceedings of 3D-ARCH 2009*.
Rusinkiewicz, S. and Levoy, M. (2001). "Efficient variant of the ICP algorithm." *Proceedings of the 3rd International Conference on 3D Digital Imaging and Modeling, 3DIM 01*, Quebec City, Canada.
Rusu, R. B., Marton, Z. C., Blodow, N., Dolha, M., and Beetz, M. (2008). "Towards 3D point cloud based object maps for household environments." *Robotics and Autonomous Systems*, 56(11), 927

– 941.
Shi, P., Robinson, G., and Duncan, J. (1994). "Myocardial motion and function assessment using 4D images." *Proceedings of Visualization in Biomedical Computing, VBC 94*, Rochester, USA.
Silberman, N., Hoiem, D., Kohli, P., and Fergus, R. (2012). "Indoor segmentation and support inference from RGBD images." *Computer Vision ECCV 2012*, A. Fitzgibbon, S. Lazebnik, P. Perona, Y. Sato, and C. Schmid, eds., Vol. 7576 of *Lecture Notes in Computer Science*, Springer Berlin Heidelberg, 746–760.
Srinivasa, S., Ferguson , D., Vandeweghe, J. M., Diankov, R., Berenson, D., Helfrich, C., and Strasdat, K. (2008). "The robotic busboy: Steps towards developing a mobile robotic home assistant." *International Conference on Intelligent Autonomous Systems* (July).
Stamos, I. and Allen, P. (2000). "3-D model construction using range and image data." *Proceedings of the IEEE Conference on Computer Vision and Pattern Recognition*, Vol. 1, 531 –536 vol.1.
Valero, E., Adán, A., and Cerrada, C. (2012a). "Automatic construction of 3D basic-semantic models of inhabited interiors using laser scanners and RFID sensors." *Sensors*, 12(5), 5705–5724.
Valero, E., Adán, A., and Cerrada, C. (2012b). "Automatic method for building indoor boundary models from dense point cloud collected by laser scanners." *Sensors*, 12(12), 16099–16115.
Valero, E., Adán, A., Huber, D., and Cerrada, C. (2011). "Detection, modeling and classification of moldings for automated reverse engineering of buildings from 3D data." *Proceedings of the 28th International Symposium on Automation and Robotics in Construction. ISARC 2011*.
Wandel, M. R., Lilienthal, A., Duckett, T., Weimar, U., and Zell, A. (2003). "Gas distribution in unventilated indoor environments inspected by a mobile robot." *Proceedings of the IEEE International Conference on Advanced Robotics (ICAR 2003)*, Coimbra, Portugal.
Wang, C., Cho, Y. K., and Kim, C. (2015). "Automatic BIM component extraction from point clouds of existing buildings for sustainability applications." *Automation in Construction*, 56, 1–13.
Wang, J. and Oliveira, M. (2002). "Improved scene reconstruction from range images." *Eurographics*, 21(3), 521–530.
Xiao, J., Owens, A., and Torralba, A. (2013). "Sun3d: A database of big spaces reconstructed using sfm and object labels." *Computer Vision (ICCV), 2013 IEEE International Conference on*, 1625–1632 (Dec).
Xiong, X., Adán, A., Akinci, B., and Huber, D. (2013). "Automatic creation of semantically rich 3D building models from laser scanner data." *Automation in Construction*, 31, 325–337.